frontiers | Frontiers in Earth Science

TYPE Original Research
PUBLISHED 02 April 2025
DOI 10.3389/feart.2025.1513588

OPEN ACCESS

EDITED BY
Christophe Pascal,
Ruhr University Bochum, Germany

REVIEWED BY
Linda Pastero,
University of Turin, Italy
Umar Ashraf,
Yunnan University, China

*CORRESPONDENCE
Han Chao,
hanxt13579123@126.com

RECEIVED 18 October 2024
ACCEPTED 04 February 2025
PUBLISHED 02 April 2025

CITATION
Yazeng M, Heping F, Hong X, Zuozhen H, Jinxiong L and Chao H (2025) Characterization and genesis mechanism of dolomite from Xike 1 well, Xisha Islands—constraints from Mg isotopes. *Front. Earth Sci.* 13:1513588. doi: 10.3389/feart.2025.1513588

Characterization and genesis mechanism of dolomite from Xike 1 well, Xisha Islands—constraints from Mg isotopes

Ma Yazeng[1], Fu Heping[2], Xu Hong[3,4], Han Zuozhen[1], Luo Jinxiong[5] and Han Chao[1]*

[1]College of Earth Science and Engineering, Shandong University of Science and Technology, Qingdao, Shandong, China, [2]PetroChina Changqing Oilfield Company, Xian, China, [3]The First Institute of Oceanography, Ministry of Natural Resources of China, Qingdao, Shandong, China, [4]Qingdao Institute of Marine Geology, China Geological Survey, Qingdao, Shandong, China, [5]School of Geosciences, Yangtze University, Wuhan, China

Dolomite is widely developed in the Xisha Islands, and there are numerous views on its genesis, with no uniform understanding at present. In this paper, the formation mechanism of dolomite of the Xike 1 well in the Xisha Islands was investigated on the basis of the petrological and geochemical characterization of core samples using experiments such as thin section identification, cathodoluminescence, scanning electron microscopy, electron microprobe, X-ray diffraction, and Mg isotope testing. The results show that (1) most of the dolomite is distributed along the weathering exposure surface with a residual structure. Dolomite without residual structures has a fog-centered bright edge with straight authomorphism or semi-authomorphism, curved surface dominated, and the degree of authomorphism controlled by the growth space; (2) the overall ordering of dolomite in the whole well is low, with an average value of 0.53, and there is little difference in ordering at different depths, the Mn and Fe contents of middle- and shallow-depth dolomites are generally low, and cathodoluminescence is not obvious; for the deep layers, the Mn and Fe contents increased by hydrothermal action, and bright yellow and orange cathodoluminescent bands were formed; (3) changes in the Mg isotopic composition of dolomite along the stratigraphic sequence of the profile are generally consistent with changes in the depositional cycle. Based on the spatially varying trajectories of δ^{26}Mg isotope profile sequences, the results indicate the presence of evaporative lagoon infiltration reflux, mixed water, and geothermally driven hydrothermal dolomitization mechanisms since reef formation.

KEYWORDS

Xike 1 well, dolomite, orderliness, Mg isotopes, dolomitization mechanism

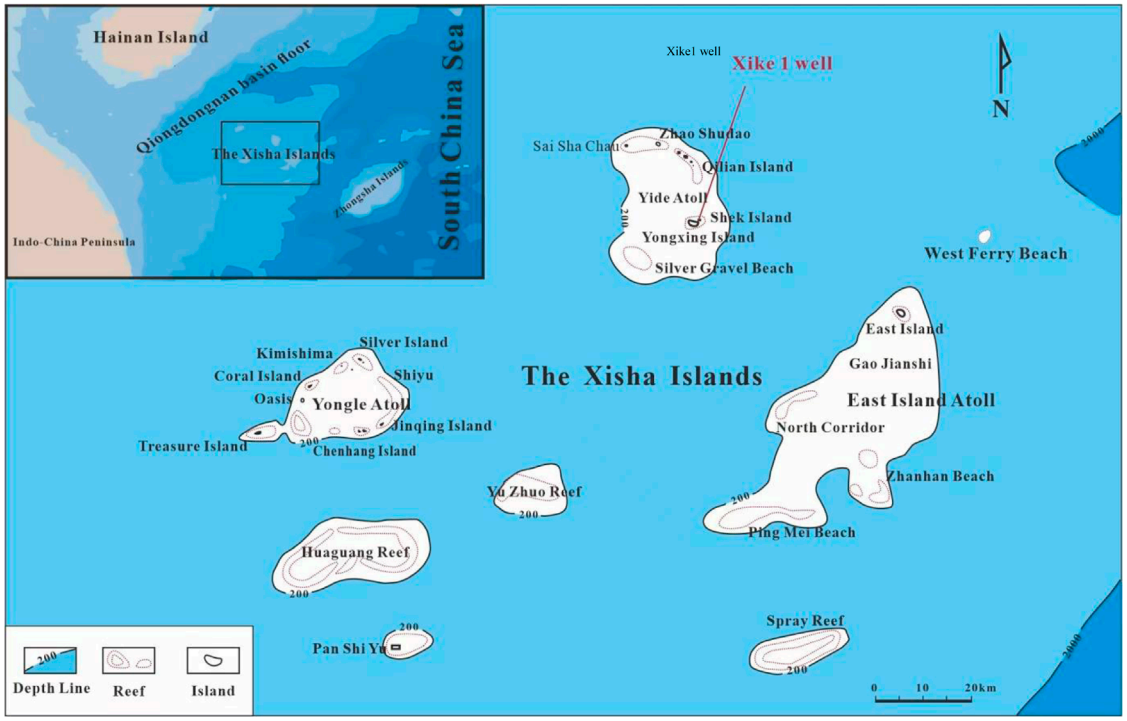

FIGURE 1
Location of the Xike 1 well, Xisha Islands.

1 Introduction

The Xisha Islands (111°-113°E, 15°30′-17°N) are located on the continental slope in the northwestern part of the South China Sea (Wang, 2001), with a total island area of 8 km^2 (Zhu et al., 2015). These islands are located in the carbonate plateau of the Xisha uplift zone, which is connected to the Qiongdongdong Basin to the north-northwest, and are atolls, developing a typical biological reef system. The study samples were mainly taken from the Xike 1 well on Xuande Atoll Rock Island, Xisha Islands (Figure 1), which was drilled in stratigraphy mainly of the Neoproterozoic system, and the rock types were mainly reef tuffs, bioclastic tuffs, and dolomites. The acquired 1,257.52 m cores of carbonate biogenic reef and beach deposits revealed that the distribution of limestone and dolomite is characterized by obvious cyclothemicity with an average coring rate of more than 85% (Luo et al., 2018). The Xike 1 well is currently the thickest and most complete core sample of bioherms revealed in the Xisha region. The encountered strata are primarily of Neogene age, with lithologies including reef limestone, bioclastic limestone, and bioreef dolomite. Notably, the dolomitic layers reach a thickness of more than 400 m, and the distribution of limestone and dolomite exhibits distinct cyclicity. Consequently, the study of this well provides a significant reference value for hydrocarbon exploration in the South China Sea block while also offering theoretical insights for research on Neogene carbonate rocks.

The dolomite of the Xike 1 well in the study area was previously assumed to be mostly formed due to the lowering of sea level to form a lagoonal environment, which triggered the mechanism of back penetration and seepage of high Mg brine (Zhai et al., 2015; Cao et al., 2016; Xiu et al., 2017; Ashraf et al., 2020; Ashraf et al., 2022; Ashraf et al., 2024; Ullah et al., 2022). In addition, thermal fluid upwelling caused by tectonic movements at the end of the Miocene contributed to the dolomitization process (Wei et al., 2018; Wang et al., 2015; Yin et al., 2020; Yang et al., 2024; Lin et al., 2024a; Lin et al., 2024b). Xu et al. (2018), Xu et al. (2021), and Wang et al. (2020) noted that dolomite in the Xike 1 well was formed under a dual diagenetic mode of osmotic reflux and geothermal warming and that hydrothermal fluids carrying manganese-bearing materials upwelled along the faults to modify the formed dolomite by diffusion. However, below the exposed surface of the Xisha Islands, there is significant hydrochemical stratification of freshwater and seawater, forming freshwater lenses, and mixing of freshwater and seawater in dissolution pore space to guide dolomitization (Xu et al., 2021; Shi et al., 2010) indicated that the formation of dolomite in the Xike 1 well may be related to microorganisms. In addition, with the development of isotope geochemical tests, Mg isotopes have gradually become a new means of studying dolomitization, which can not only indicate the source of Mg but also the direction of fluid transport through its spatial variation (Ning et al., 2020; Han et al., 2023; Dong et al., 2024). Currently, previous research on the genesis of dolomite in Well Xike 1 has predominantly focused on aspects such as petrography, paleontology, and elemental geochemistry. However, there is a lack of sufficient research regarding Mg isotope geochemical characteristics.

In this paper, the formation mechanism of dolomite of the Xike 1 well in the Xisha Islands was investigated on the basis of the petrological and geochemical characterization of the core samples using experiments such as thin section identification,

cathodoluminescence, scanning electron microscopy, electron microprobe, X-ray diffraction, and Mg isotope testing. Ultimately, multiple mechanisms for the existence of dolomitization effects in the Xisha Islands since reef formation were elucidated.

2 Geology section and methods

The drilling site of Well Xik-1, Shidao, is located at the northeastern corner of Yongxing Island in the Xishaipelago on the carbonate platform developed on the Xisha Block since the Neogene. The Xike 1 well is a fully developed biotic reef carbonate rock with the underlying rock type changing from carbonate rock to volcanic and metamorphic rocks forming the basement. The sedimentary sequence above the basement is continuous and complete, including stratigraphic units such as the Lower Miocene, Middle Miocene, Upper Miocene, Pliocene, and Quaternary, which include the Sanya Formation, Meishan Formation, Huangliu Formation, and Yinggehai Formation.

Multiple sections of dolomite are developed in the Xike 1 well, and the distribution of calcite and dolomite is distinctly cyclostratigraphic, with the developed crystalline dolomite having a hard texture that is easily distinguishable from weakly consolidated white limestones that are poorly densified. Thick-bedded dolomite is mainly concentrated in the second member of the Yinggehai Formation (296.98~303.35 m), Huangliu Formation (375.69~572.25 m), the first member (620~645.5 m), the second member (758.09~774.8 m) and the third member of Meishan Formation (971.66~1,036.58 m), and the first member of Sanya Formation (1,044.13~1,173.62 m), and a small amount of dolomite is also distributed in the second member of the Sanya Formation (Figure 2). All test samples covering these formations were completed in September 2020 with targeted sampling in the Zhanjiang area, the cores taken started at 375 m up to the gneiss basement, and the samples were dominated by dolomite.

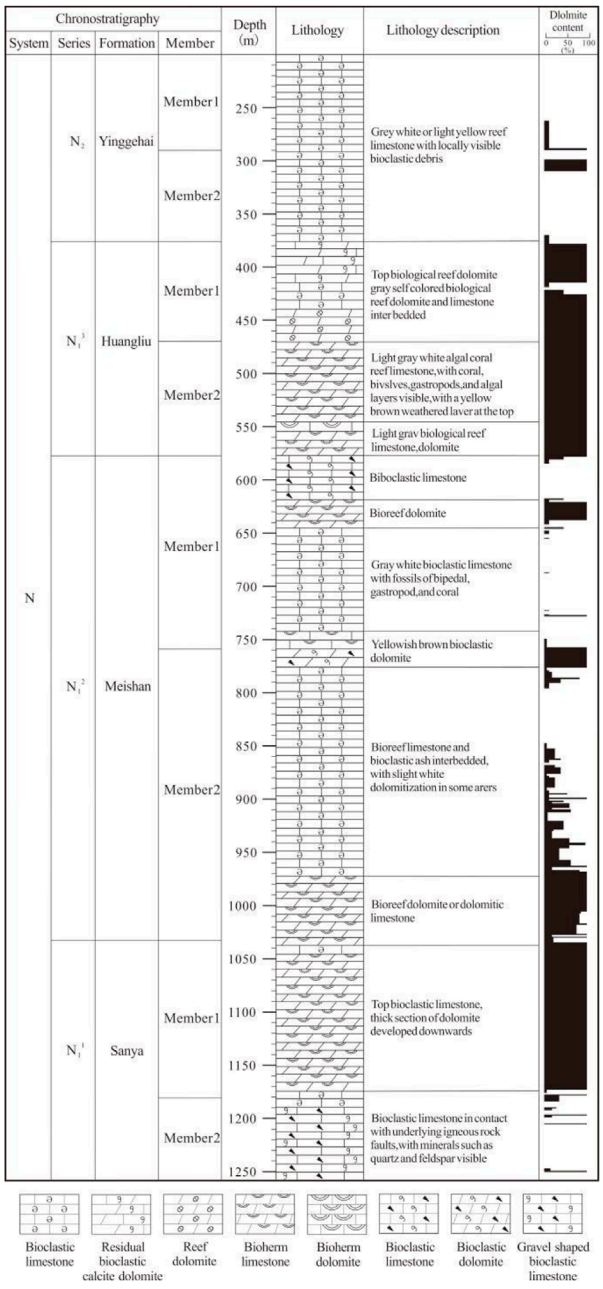

FIGURE 2
Comprehensive histogram of the stratigraphy of the Xike 1 well (dolomite content referenced from Wang et al., 2020).

2.1 Major element test

Acid dissolution (HF + HNO_3) was used to dissolve the samples, and inductively coupled plasma spectrometry (ICP-OES) was used to test for the major elements. The samples were dissolved by acid dissolution (HF + HNO_3), and international standard samples (GSR-5, GSR-6, and GSD-9) and blank samples were used for calibration during the dissolution process. An inductively coupled plasma spectrometer (ICP-OES) was used to test the principal elements Al, Fe, Ca, Na, K, Mg, P, and Sr. The working curves were established by using the international single-element standard, and the correlation coefficients of the working curves for each element were all above 0.99999, with the relative standard deviations (RSDs) of Al, Fe, Ca, Na, K, Mg, P, and Sr less than 0.5%, and the RSD of element P less than 1%.

2.2 Mg isotope test

Determination of Mg isotopes was accomplished using a Neptune Plus type multi-receiver inductively coupled plasma mass spectrometer (MC-ICP-MS) at the Laboratory of Metal Stable Isotope Geochemistry, University of Science and Technology of China. Depending on the Mg content, powder samples of approximately 100 mg were prepared. A measure of 5–20 mg of sample powder was weighed and fully dissolved to obtain approximately 20 μg Mg for chemical purification. The separation was treated with concentrated HF + HNO_3 (3:1, v/v) for dissolution. After initial dissolution and evaporation to dryness, the samples were treated with aqua regia and dried again, and the samples were then refluxed with concentrated nitric acid to remove residual fluoride and finally dissolved in 1 mL of 2 N HNO_3 in

preparation for column chemistry. Mg purification was performed in Savillex microcolumns (6.4 mm I.D. × 6.2 cm bed height, 30 mL reservoir) loaded with 2 mL Bio-Rad AG50W-X12 (200–400 mesh) cationic resin. Mg isotope measurements were carried out using the sample-labeling crossover method (Ning et al., 2018). The sample volume of this test was 40 μg, and the blank of the whole process was no more than 22.6 ng, and the blank effect was no more than 1‰; the sample recovery was better than 99.5%.

The Mg isotope value is expressed as a thousandth difference from the standard sample:

$$\delta^{x}\mathrm{Mg} = \left[\left({}^{x}\mathrm{Mg}/{}^{24}\mathrm{Mg}\right)_{\mathrm{Sample}}/\left({}^{x}\mathrm{Mg}/{}^{24}\mathrm{Mg}\right)_{\mathrm{Standard}} - 1\right] \times 1000\,(‰),$$

where $x = 25, 26$.

2.3 *C/O* isotope test

C/O isotope measurements were accomplished using an Isotope Ratio Mass Spectrometer (DELTA V Advantage SN09017D) at the Experimental Center of the School of Geosciences at Yangtze University. The experimental steps included (1) fine grinding of the samples using a laboratory agate bowl, crushing the samples under a microscope, and washing them three times in ultrasound using alcohol at a concentration of 99.7% or higher for 5–10 s each time to ensure cleanliness and purity of the samples. (2) The samples are dried in an oven for 5 h. (3) The samples were processed and transferred to a Finnigan automated calcium carbonate sampling device (Kiel Model III) to react with the original phosphoric acid to produce carbon dioxide. (4) Measurement of oxygen–carbon isotope values of collected carbon dioxide gas using a Finnigan Model MAT252 Stable Isotope Mass Spectrometer. The Chinese national standard for calcium carbonate (GBW04405) and the international standard (NBS19) were used as benchmarks during the tests, and standard errors of 0.03‰ and 0.14‰ were calculated.

Cathodoluminescence, electron microprobe, and XRD tests were done at the CNOOC Experimental Center, Engineering and Technology Company, CNOOC Energy Development Co. SEM was tested at the Qingdao Institute of Marine Geology. Mg isotopes were tested by the Laboratory of Metal Stable Isotope Geochemistry, University of Science and Technology of China.

3 Results

3.1 Distributional characteristics of dolomite profile sequences

The shallowest dolomite was found to be distributed at 375 m in a section of the Huangliu Formation of the Upper Miocene, and this section of dolomite was white and light grayish-white; the dolomite samples were poorly consolidated, with small specific gravity; and the weathering exposure surface was obvious. White powder falls off the surface of the central mid-depth dolomite sample. Dolomitization is significantly enhanced at 620~645.5 m (first member of the Meishan Formation), with a good degree of consolidation, high specific gravity, and densely distributed surface pores. For 758.09~774.8 m (the second member of the Meishan Formation) cores, dolomite appears as dark gray and yellow-brown, which is mainly large-segmented blocky hard dolomite, and the dolomite is sandy-sugar-like, crystalline dolomite with a good degree of solidification, as observed by the naked eye. The lower deep dolomite is well-cemented. For 971.66~1,036.58-m (the second member of the Meishan Formation) cores, the dolomite content profile sequence is jagged and fluctuating, with only localized dolomitization, an average degree of consolidation, light specific gravity, and uneven surface of the core, with very well-developed biogenic relics, as well as biogradient support. For 1,044.13~1,173.62 m (the first member of the Sanya Formation), dolomite generally displays light grayish maroon, brown, or brown color; is well-cemented; and has a high specific gravity. It is topped by a distinctly weathered layer with the development of brown irregular bands. After 1,138 m, the core develops a large number of "almond-shaped" regular intergranular pores. Sugar-grained sandy feelers are very evident at the base, and the non-dolomitic sections are weakly consolidated and broken at the base. The second member of the Sanya Formation is a brick-red breccia, and breccia is grayish-white and haphazardly distributed in the brick-red matrix (Figure 2), with quartz, feldspar, and other minerals identified by XRD tests.

Residual biotite dolomite is extensively developed in the Xike 1 well and includes fossilized calcareous algae and corals, as well as echinoderms, foraminifera, and other detritus. Due to strong dolomitization, most bioclastic primitive biofossil features are obscured. The proportion of dolomite without a residual structure is small, the fog-centered bright edge structure is common, well-crystallized rhombohedrons are developed, and microcrystalline-powder-crystalline dolomite has a tendency to become larger crystals with increasing depth. Influenced by the increase in stratigraphic temperature, the greater the burial depth, the easier it is for dolomite to recrystallize and form larger grains (Tong et al., 2023). Dolomite exhibits two kinds of endowment mode, either in the form of collodion filled in the pore space or accounted for biological debris endowed in the particles. Due to the progression of continuous supply of dolomitized fluids, pore dolomite comprises mainly bright crystals with a good crystal shape but rarely fills the pore completely. The crystal shape is mainly controlled by the recrystallization action and the growth and development space; when the growth space is limited, the mosaic contact and step growth are dominated, and the dolomite crystals are also transitioned from autoclave to semi-autoclave and iteromorphic shape. Referring to the classification scheme of Sibley and Gregg (1987), dolomite is classified into three categories by considering the shape of the dolomite crystals and boundary characteristics, taking the medium-depth-deep dolomite as an example: straight-surface authomorphic or semi-authomorphic dolomite, curved-iteromorphic dolomite, and curved-surface saddle-shaped dolomite (Figure 3).

Electron microprobe testing plays a vital role in studying the chemical composition of dolomite. Electron microprobe tests show that dolomite crystals are not uniformly dolomitized. Not only are different crystal elements not the same, but the same dolomite crystals also have different elements. The MgO content in the center of dolomite crystals is generally lower than that

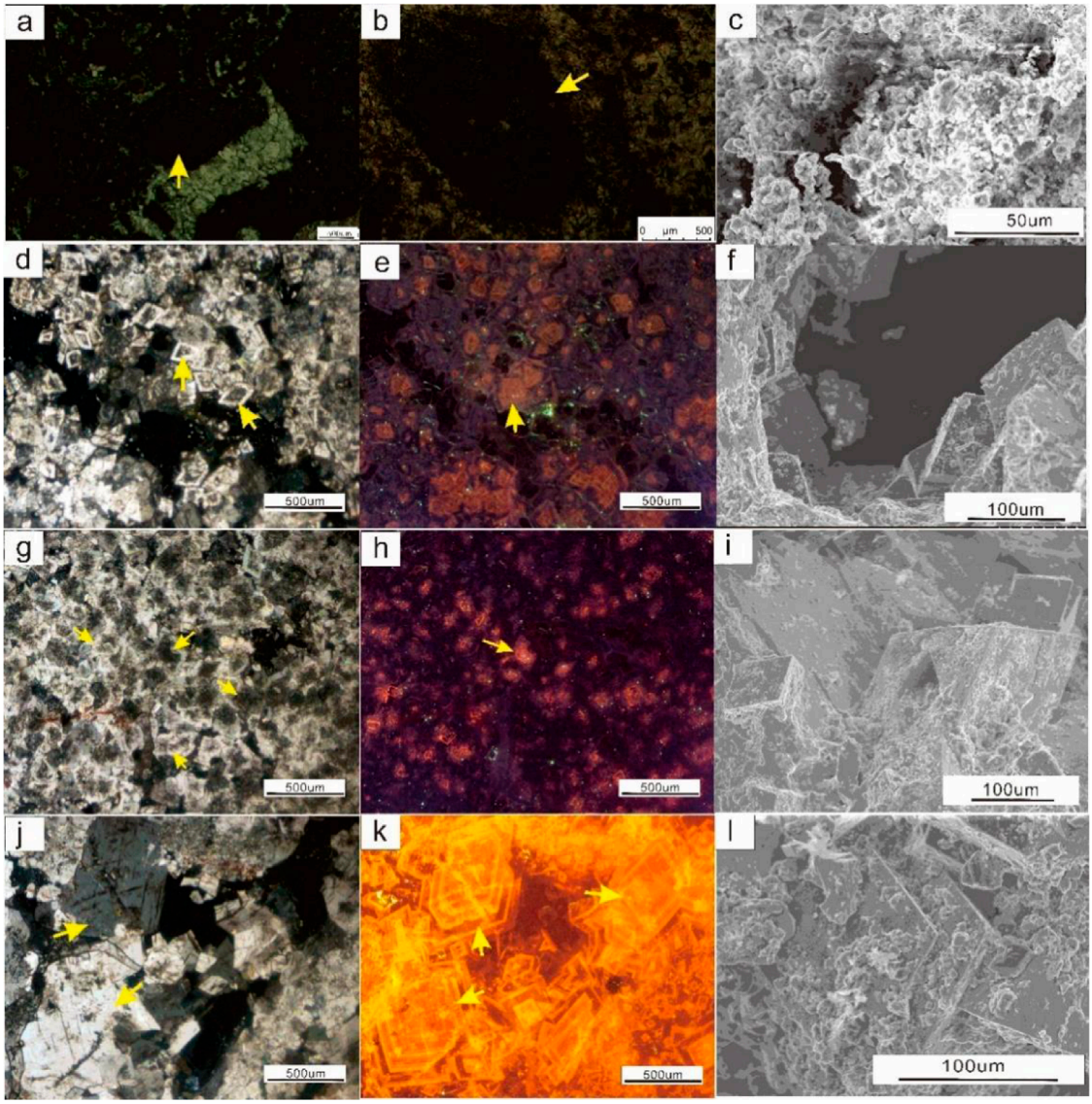

FIGURE 3
Microscopic characteristics of different types of dolomites in the Xike 1 well: **(A)** at 740.34 m, complete nephrolepis is visible and dolomite is developed in holes, with single polarized light; **(B)** at 1,138.03 m, algal grains with detritus, filled with mud-crystalline calcite or dolomite, surrounded by development of fog-centered bright-edged dolomite, were observed as stained flakes; **(C)** at 375.89–375.95 m, mud powder crystal dolomite is observed via SEM; **(D)** at 747.39–747.54 m, for straight-sided authomorphic or semi-authomorphic dolomite, fog-centered bright rims developed, as indicated by yellow arrows via orthogonal light; **(E)** cathodoluminescence photograph with **(D)** in the same field of view, where fine-crystalline dolomite glows red; **(F)** at 745.87–745.97 m, dolomite cemented along pores, SEM, **(G)** 1,053.90–1,053.95 m, curved iteromorphic dolomite is observed, as indicated by the arrowheads, with a distinct fog-centered bright-edge structure, orthogonal light; **(G, H)** have the same field of view, part of the dolomite luminescence and show alternating light and dark ring bands via cathodoluminescence; **(I)** at 1,254.00 m, fog-centered dissolved dolomite crystals are observed via SEM; **(J)** 1257 m, saddle-shaped dolomite, well-developed internal micro-cracks, wavy extinction, orthogonal light; **(J, K)** have the same field of view, and the saddle-shaped dolomite shows a clear bright yellow and orange alternating ring band via cathodoluminescence; **(L)** at 1,254.00 m, step-growth dolomite, SEM.

at the edges of the crystals. Such dolomite fine crystals are generally haze-centered bright-edge dolomite, whose haze-centers have a slightly lower Mg content and a slightly higher Ca content than bright-edge dolomite (Figures 4A–D), which shows the difference in the degree of crystallization of dolomite. In other words, the dolomite crystal centers are less dolomitized than the edges, and the center has a residual structure. The dolomite has low values of Fe and Sr, and Si and Mn are only abundant at the base.

3.2 Orderliness characteristics of dolomite

The Xike 1 well developed multiple sections of dolomite, and two samples were taken from a section of the Huangliu Formation from 377.64 to 415.39 m. Although the degree of consolidation was weak and the hardness was low, tests revealed that the dolomite content was more than 95%. The first and second members of the Huangliu Formation from 424.98 to 572.25 m develop thick-bedded dolomite with the dolomite content greater than 93% and

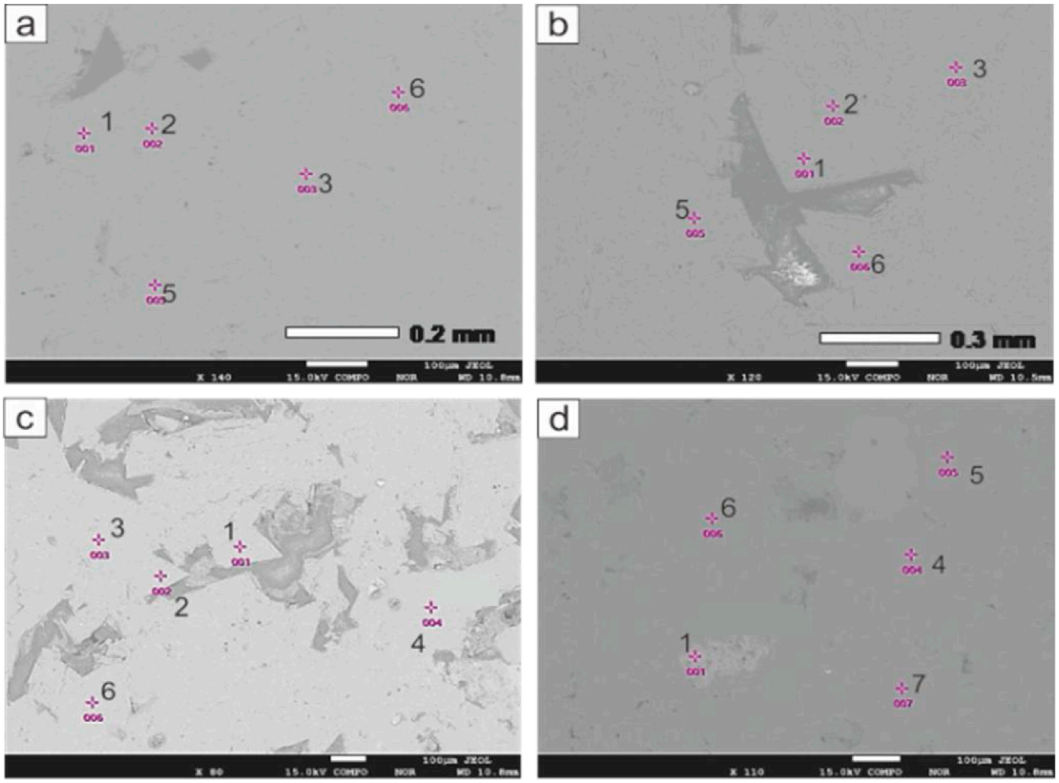

FIGURE 4
Electron microprobe analysis of dolomite crystals from the Xike 1 well: **(A)** Sample depth 1,100.15~1,100.21 m. Point 1 is located at the edge of rhodochrosite crystals with 13.77% Mg content, and Point 2 is located at the center of rhodochrosite crystals with 12.66% Mg content. **(B)** Sample depth 1,169.86~1,170.02 m. Point 1 is located at the edge of rhodochrosite crystals with 13.78% Mg content, and Point 2 is located at the center of rhodochrosite crystals with 12.91% Mg content. **(C)** Sample depths 1,254.07 ~ 1,254.13 m. The location of Point 4 is quartz. **(D)** Sample depth 1,257.30–1,257.38 m. Point 1 location is manganese nodule.

a small amount of calcite. Eight samples were taken from the first member of the Meishan Formation from 620 to 645.5 m, with a high degree of consolidation under the hand specimen. Moreover, X-ray powder crystal diffraction physical analysis shows that the dolomite content is predominant, and a section of dolomite of approximately 25 m thick is developed in this section, with the calcite content becoming more abundant at 646 m. The dolomite content in this section is approximately 1 m thick. The samples at 734.80~747.00 m are dominated by calcite, but the degree of consolidation is high and hardness is high under the hand specimen, and thin layers of dolomite are developed in individual places without forming thick layers of dolomite, and bioclastic debris is abundant in the section under the polarized light microscope. Dolomites are developed at 758.09~774.8 m of the second member of the Meishan Formation, including thin dolomite, authigenic, semi-authigenic, and iteromorphic dolomite. Dolomite crystals with complete crystal faces are seen under a scanning electron microscope. The second section of the Meishan Formation from 971.66 to 1,036.58 m contains more calcite than dolomite developed in other layers, showing that its dolomitization is incomplete. The polarized light microscope shows abundant pores with de-dolomitization. For the first member of the Sanya Formation from 1,044.13 to 1,173.62 m, thick layers of dolomite are developed with more than 95% dolomite content. Fog-centered bright edge features are obvious, and semi-autoclastic to italic structures are developed. After 1,173 m, due to the contact with the gneiss basement, the minerals such as quartz and feldspar are increased by its influence. Diffraction patterns show multiple phases, for example, at 1,235 m, X-ray powder diffraction identified not only dolomite but also quartz (Figure 5). Although dolomite is developed, it is only in thin layers and saddle dolomite is developed.

The relatively strong I (015)/I (110) ratio on the X diffraction pattern characterizes the magnitude of ordering. The ratio ranges from 0 to 1, and the closer it gets to 1, the better the ordering and the more regular the crystal arrangement. The average dolomite orderliness of 375.69~572.25 m of the Huangliu Formation is 0.52; the average dolomite orderliness of the first member of the Meishan Formation, 620~645.5 m, is 0.54; the average dolomite orderliness of the second member of the Meishan Formation, 758.09~774.8 m, is 0.48; the average orderliness of the first member of the Meishan Formation, 971.66~1,036.58 m, is 0.52; the average orderliness of the first member of the Sanya Formation, 1,044.13~1,173.62 m, is 0.53, while the first member of the Sanya Formation, 1,044.13~1,173.62 m, has an average orderliness of 0.53. The five members of thickly bedded dolomite developed from the Huangliu Formation to the Sanya Formation neither differ much in their orderliness nor do they show any adjustment

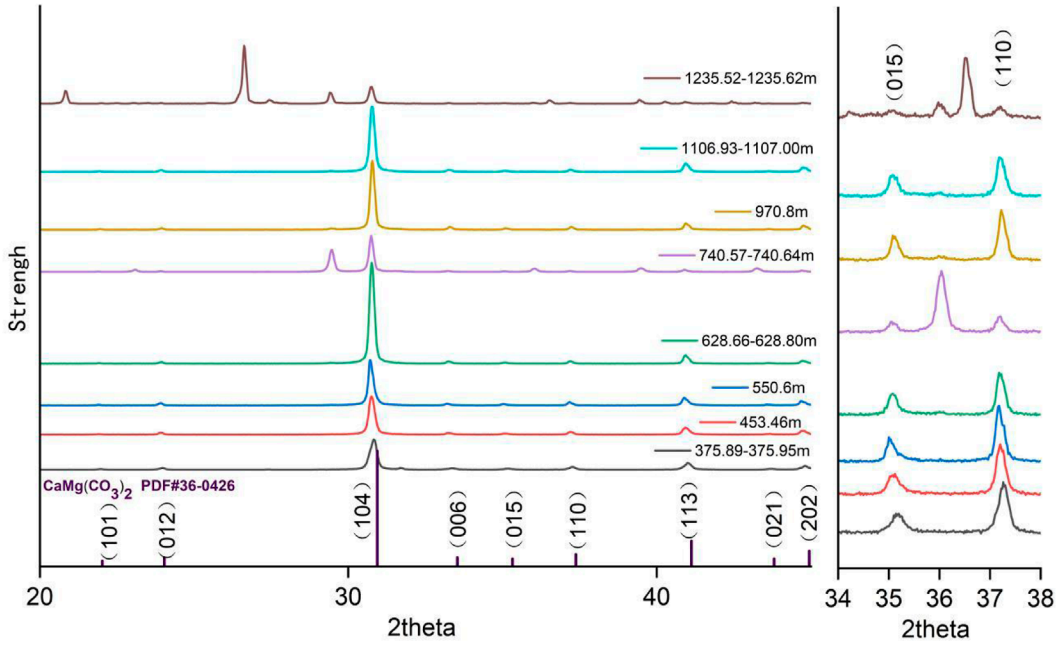

FIGURE 5
X-ray diffraction results of dolomite from the Xike 1 well.

of orderliness with depth. The basal dolomite is sporadically distributed, and its ordering is high due to hydrothermal influences.

Different mineral phases have different characteristic diffraction peaks in the X-powder crystal diffraction pattern, and the types of their main mineral phases are judged according to their diffraction peaks and the different angles at which they are located. According to the different diffraction intensities and positions of the calcite (104) and dolomite (104) characteristic peaks, calcite and dolomite minerals can be qualitatively analyzed from the X-powder crystal diffraction patterns. The XRD diffraction curves at 375.89~375.95 m, 453.46 m, and 550.6 m of the Huangliu Formation (104) have characteristic peaks d between 2.854 and 2.912 Å and are dolomite minerals. The XRD diffraction curves at 628.66~628.80 m and 970.8 m of the Meishan Formation also show dolomite. The minerals are mixed dolomite and calcite from 740.57 to 740.64 m. The minerals of the Sanya Formation from 1,106.93 to 1,107.00 m are dolomite, and the X-ray powder diffraction of the Sanya Formation from 1,235.52 to 1,235.62 m recognizes not only dolomite but also quartz.

There is no significant correlation between the degree of dolomite ordering and the average grain size with depth. The ordering of dolomite is low overall, and there is very little difference in the ordering of different groups of dolomite (Figures 6A–D). The bottom boundary of the dolomite in a section of the Meishan Formation is incompletely dolomitized due to reduced fluid supply, and unaccounted-for red calcite is seen under stained slices (Figure 6B), and the degree of ordering is low compared to the top boundary. The dolomite located in the second section of the Meishan Formation from 758.09 to 774.8 m is exactly the opposite, with red calcite seen at the top boundary under the stained thin section, and the degree of ordering is lower than that of the lower boundary (Figure 6C). It suggests that these two sections of dolomite formed in different fluid environments. The dolomite in the second member of the Sanya Formation is affected by hydrothermal fluids, and some of the ordering degrees are high, such as the dolomite at 1,230 m with an ordering degree as high as 0.89.

3.3 Isotopic characterization of dolomite

The elemental results of the samples are shown in Table 1, with an average of 38.72% CaO and 14.67% MgO. The low MgO content of the sample located at approximately 646 m (ordering degree 0.16) and the sample located at approximately 747 m (ordering degree 0.45), as well as the low MgO content of some of the samples, indicate that only weak dolomitization occurs. By XRD analysis, the main component of all these samples is dolomite, and the difference is only the difference in the degree of dolomitization. Samples with weak dolomitization are poorly ordered, have low MgO content, and microscopically show mostly reddish calcite by observing potassium ferricyanide and alizarin red S-stained thin sections.

The standards used for the Mg isotope testing experiments were BIR-1 and AGV-2, and the measured isotope results were in agreement with the results of previous data within the error range (Table 2).

The sample test results showed a mean value of −3.56‰ with a wide range of variation from −4.05 to −3.04‰. The test results show that the dolomite samples are more enriched in lighter Mg isotopes, with no correlation with age. Mg isotope sample Huangliu Formation 550.6 m, $\delta 26Mg = -3.89$, Meishan Formation 620~645 m

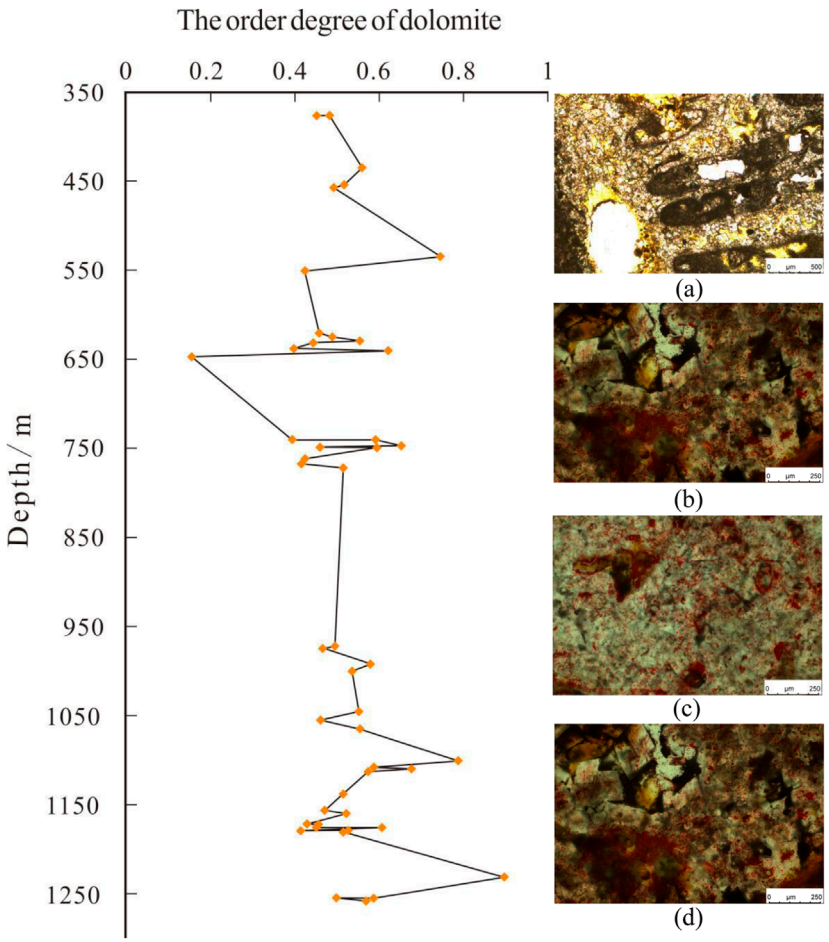

FIGURE 6
Variation n dolomite orderliness with depth: **(A)** 453.46 m, bioclastic debris remnants; **(B)** 639.89–639.94 m, dolomite bottom boundary of the first member of the Meishan Formation, with incomplete dolomitization and stained flakes; **(C)** 740.57–740.64 m, dolomite top boundary of the second member of the Meishan Formation, with incomplete dolomitization; **(D)** 1,109.72–1,109.77 m, fog-centered bright-edged dolomite.

δ26Mg variation range between −4.05 and -3.01‰; the range of δ26Mg variation is large and decreases with depth; in the depth of 758.09~774.8 m sampling of three points, the δ26Mg values are −3.64‰, −3.83‰, and −3.90‰, respectively; the depth of 971.66~1,036.58 m has only two points, namely, −3.61‰ to −3.60‰; for 1,044.13~1,173.62 m, the δ26Mg value varies from −3.04‰ to −3.93‰, with a wide range, and the δ26Mg value of dolomite is the largest at approximately 1165 m.

4 Discussion

4.1 Diagenetic alteration

Mn/Sr values of carbonate rocks increase with increasing diagenetic alteration, and samples are considered to have been subjected to weak diagenetic alteration when their Mn/Sr values are <3 (Kaufman et al., 1993; Kouchinsky et al., 2008). The value of carbonate rocks decreases with the enhancement of diagenetic alteration, and when the $\delta^{18}O$ value is <-10‰, the carbonate rock suffers from strong diagenetic alteration effects (Kaufman and Knoll, 1995; Li et al., 2009).

The test samples $\delta^{26}Mg$ and $\delta^{25}Mg$ fall on the mass fractionation line (Figure 7A), indicating that the homogeneous isotopes can be neglected during the mass spectrometry measurements. There is no linear correlation between $\delta^{26}Mg$ and Mg/Ca (Figure 7B) so that interference of Mg isotopes by the mixing of large amounts of calcite can be excluded. In addition, no significant linear correlation exists for $\delta^{18}O$, Mn/Sr, and $\delta^{26}Mg$ (Figures 7C, D), suggesting that dolomite Mg isotopes were not subjected to alteration during diagenesis.

The Mg isotopic compositions of the dolomites are more positive than those of the chert system, with the dolomites varying from −3.25 to −0.38‰. The mean and range of variation in $\delta^{26}Mg$ of the results tested in this study are more negative than the average dolomite and have approached the calcite system. It is possible that the influence of the reef dolomite formation process involving microbial action, among other things, has made it easier for lighter Mg isotopes to enter the mineral lattice.

TABLE 1 Trace element, carbon and oxygen isotope, and Mg isotope compositions of dolomite samples from the Xike 1 well.

Sample number	Depth	CaO	MgO	Mg/Ca	Mn	Sr	Mn/Sr	$\delta^{13}C$	$\delta^{18}O$	$\delta^{25}Mg$	2SD	$\delta^{26}Mg$	2SD
	m	%	%	mol/mol	‰	‰		‰	‰	‰	‰	‰	‰
ISO7	550.6	40.60	17.89	0.62	7.24	243.90	0.03	—	—	−2.02	0.04	−3.89	0.05
ISO8	620.55–620.61	36.50	19.50	0.75	8.66	195.90	0.04	3.11	3.34	−2.11	0.07	−4.05	0.10
ISO11	628.66–628.80	39.40	20.59	0.73	17.43	214.50	0.08	3.22	1.42	−1.72	0.02	−3.29	0.04
ISO15	646.30–646.37	54.40	1.94	0.05	3.87	296.80	0.01	3.10	0.72	−1.56	0.03	−3.01	0.03
ISO20	747.39–747.54	54.50	1.83	0.05	8.42	889.70	0.01	2.78	1.23	−1.90	0.04	−3.64	0.05
ISO23	761.37–761.49	34.90	20.29	0.81	19.52	175.60	0.11	3.09	0.71	−1.98	0.02	−3.83	0.02
ISO25	771.9	37.30	21.18	0.80	14.72	197.40	0.07	2.86	1.19	−2.02	0.04	−3.90	0.09
ISO26	970.8	33.60	17.86	0.74	21.70	291.65	0.07	2.16	1.15	−1.88	0.04	−3.61	0.04
ISO29	998.9	48.80	4.02	0.12	18.05	361.30	0.05	—	—	−1.86	0.13	−3.60	0.25
ISO32	1,053.90–1,053.95	33.20	18.34	0.77	44.26	223.50	0.20	2.39	0.58	−2.04	0.03	−3.93	0.05
ISO33	1,063.46–1,063.53	33.00	17.76	0.75	101.27	220.20	0.46	2.66	0.36	−1.71	0.04	−3.30	0.09
ISO34	1,100.15–1,100.22	33.00	18.73	0.79	37.84	207.70	0.18	2.56	−0.23	−1.73	0.07	−3.34	0.10
ISO36	1,109.72–1,109.77	33.50	18.87	0.79	196.86	200.80	0.98	2.36	−0.99	−1.87	0.06	−3.58	0.08
ISO40	1,159.77–1,159.92	32.70	18.32	0.78	30.66	239.80	0.13	2.09	−2.35	−1.59	0.11	−3.04	0.16
ISO41	1,169.86–1,170.02	31.70	18.99	0.84	21.72	225.80	0.10	—	—	−1.65	0.07	−3.14	0.07
ISO42	1,173.27–1,173.42	32.60	17.95	0.77	33.07	243.60	0.14	2.23	−2.17	−1.82	0.02	−3.48	0.02
ISO46	1,176.8	33.20	17.98	0.76	108.75	252.60	0.43	1.99	0.05	−1.78	0.05	−3.42	0.09
ISO47	1,178.92–1,178.98	33.30	17.78	0.75	75.71	246.90	0.31	—	—	−1.85	0.01	−3.57	0.02
ISO48	1,179.52–1,179.62	51.30	1.17	0.03	25.27	477.20	0.05	—	—	−2.05	0.04	−3.99	0.04
ISO55	1,254.07–1,254.13	46.80	2.48	0.07	162.58	203.80	0.80	—	—	−1.92	0.04	−3.68	0.03

10.3389/feart.2025.1513588

TABLE 2 Analytical results and comparisons of Mg isotopes of standard samples.

Sample number	δ^{25}Mg	2SD	δ^{26}Mg	2SD	N	Recommended value
BIR-1	−0.098	0.026	−0.198	0.039	3	δ^{26}Mg = −0.216 ± 0.055 (An, Y, et al., 2014)
AGV-2	−0.077	0.019	−0.150	0.026	3	δ^{26}Mg = −0.124 ± 0.033 (An, Y, et al., 2014)

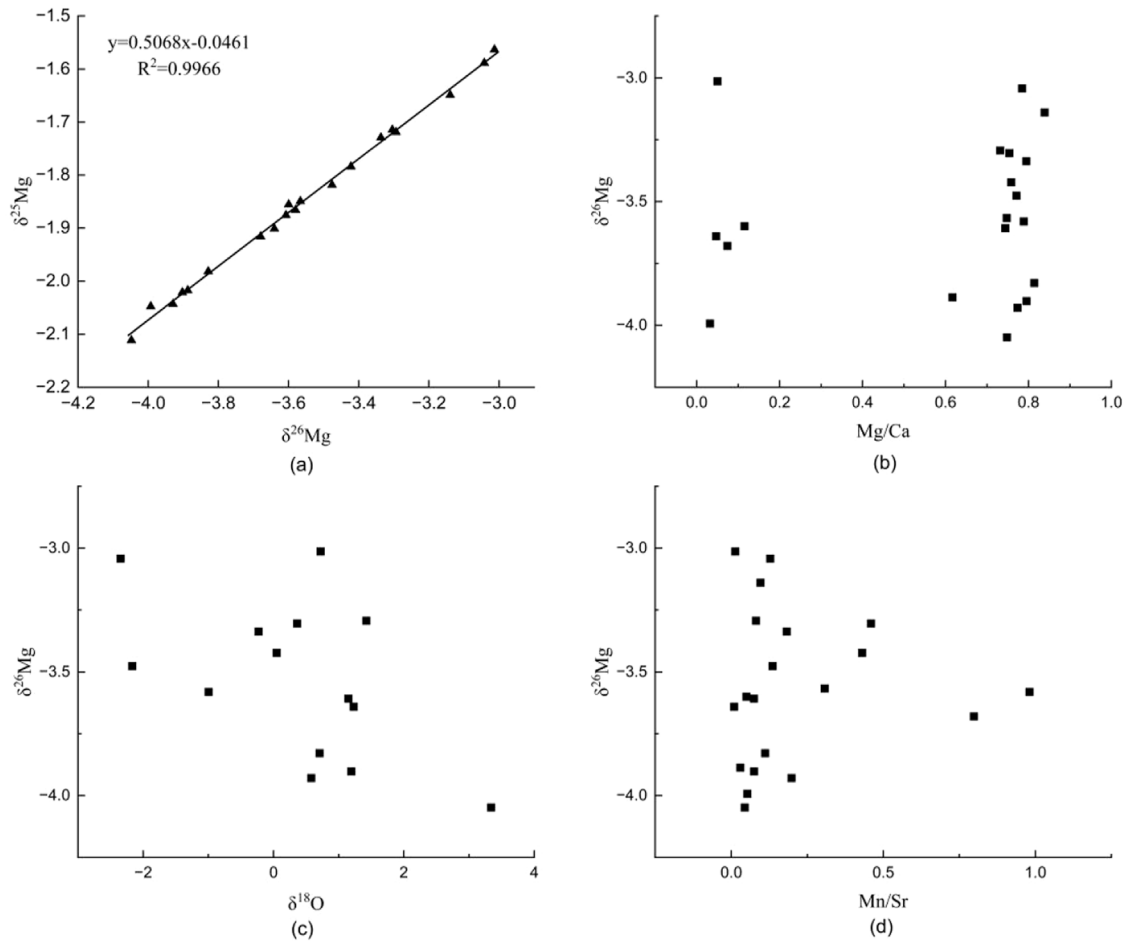

FIGURE 7
Cross plots of **(a)** δ^{26}Mg and δ^{25}Mg, **(b)** δ^{26}Mg and Mg/Ca, **(c)** δ^{26}Mg and δ^{18}O, and **(d)** δ^{26}Mg and Mn/Sr for the dolomite of the Xike 1 well.

4.2 Spatial variation in orderliness

Xisha BioReef dolomite is concentrated below the Pliocene–Pleistocene divide, below the Miocene-Pliocene hiatus, below the two hiatus surfaces of the Middle Miocene, and at the exposure between the base of the Middle Miocene and the Lower Miocene, marking the Arctic Ice Sheet Formation Event, the Messinian Event, the Antarctic Ice Sheet Expansion, and the Early Miocene Series of Cold Events (Figure 8). Sea-level rise and fall associated with paleoclimate change indirectly control dolomitization of island carbonates.

In terms of the formation rate of orderliness, dolomite orderliness in the study area is on the small side, with an average value of only 0.53, indicating that the dolomite crystals in the region have a large formation rate and belong to the orderliness of the rapid formation period. It is also possible that the addition of Fe^{2+} reduces the degree of order (Richardson et al., 2022; Xie et al., 2022). Therefore, the low degree of order cannot simply be considered to be due to the fast crystallization rate that is too late to adjust to the ordered state. More Fe ions from seawater enter the mineral lattice during dolomitization, while fewer Mn ions enter, causing cathodic luminescence to be suppressed, resulting in relatively weak luminescence in leucocrystalline-cemented dolomite and recrystallized dolomite. The second member of the Sanya Formation is affected by the basal hydrothermal fluids, and the content of Mn elements increases but the distribution is not uniform, and the dolomite in this section shows obvious bright yellow and orange alternating rings under cathodoluminescence, and the bottom of the

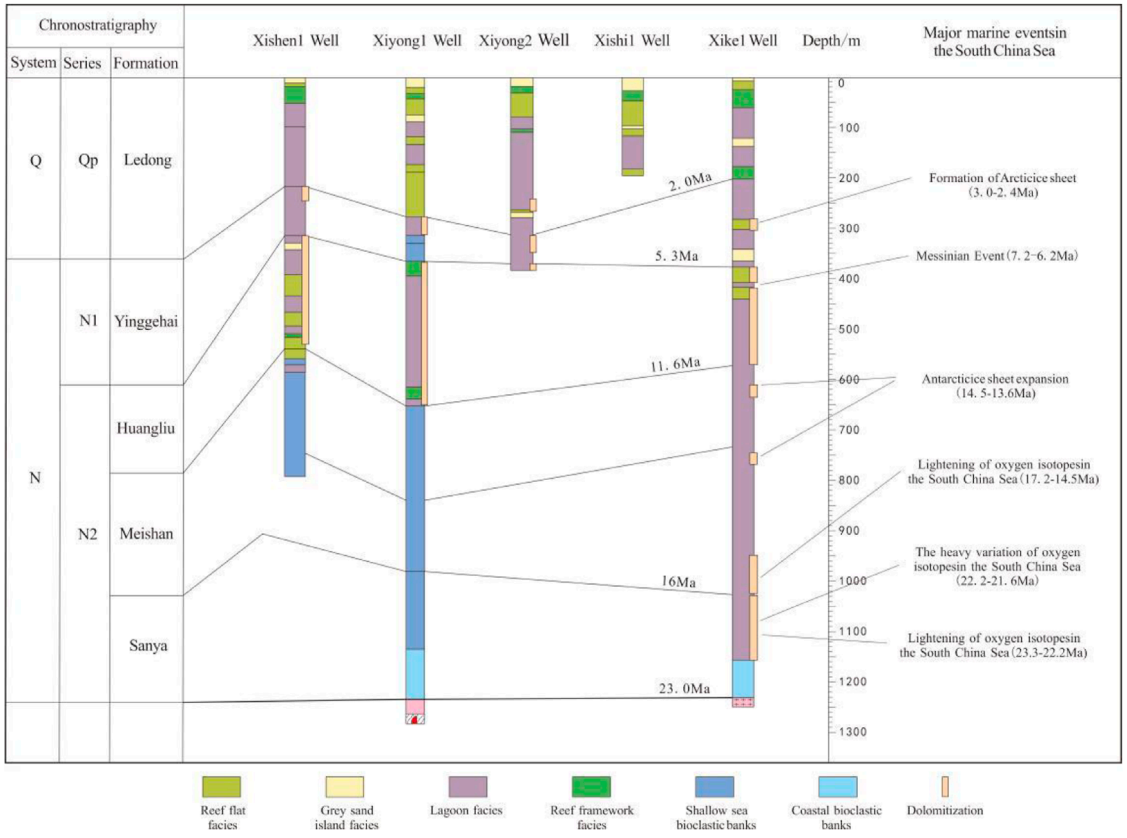

FIGURE 8
Comparison of sedimentary facies in the Xisha Sea and major events in the South China Sea.

section is affected by the high-temperature hydrothermal fluids, and the degree of dolomite ordering is relatively high.

From scanning electron microscopy and rock thin section analyses, the dolomite crystals generally develop more regular rhombic dolomite crystals, and there should be enough time and space for the dolomite growth process to form the ideal degree of crystal structure. At shallow depths, dolomite has a high degree of autoclasticity and small crystals, and its porosity is high enough to allow unrestricted space for crystal growth and development. After 620 m, the porosity of the dolomite layer section has become lower, and the crystals have gradually transformed to semi-autogenous and are iteromorphic-shaped. However, the correlation between crystal shape and orderliness of dolomite may not be so strong, and the crystal shape is mainly controlled by recrystallization and growth development space. The dolomite from 971.66 to 1,036.58 m (the second member of the Meishan Formation) has an average degree of consolidation, lighter specific gravity, more pores and fractures, and a relatively high degree of dolomite authomorphism.

4.3 Fluid flow

The flow trajectories of dolomitized fluids can be inverted using the AF model to indicate the dolomitization process (Figure 9). Due to the preferential enrichment of ^{24}Mg during dolomite formation, ^{26}Mg is gradually enriched in the dolomitized fluids as the dolomitization process progresses, resulting in higher $\delta^{26}Mg$ values for dolomites formed later. Therefore, vertical $\delta^{26}Mg$ profiles can be used to constrain the transport of Mg during dolomitization and the evolution of Mg isotopic compositions in dolomitized fluids, thus directly reflecting the dolomitization process (Li et al., 2022).

In the advective flow (AF) model, Mg^{2+} migrates through fluid flow and is used to describe dolomitization processes with fluid participation in mixed water models, reflux osmosis models, and hydrothermal models. Exploring the direction of different fluid flow transports during dolomitization through vertical variations in dolomite Mg isotope compositions can provide direct evidence of the dolomitization process, which, in turn, indicates the possibility of multi-phase spatial superposition formation of thick-bedded dolomite (Ning et al., 2020).

Based on the stratigraphic sequence stratigraphy of Xike 1 well (Liu et al., 2021) data, a comparison reveals that the variation in dolomite Mg isotopic compositions along the stratigraphic section sequence stratigraphy is broadly consistent with the variation in depositional cycles (Figure 10). The $\delta^{26}Mg$ value of dolomite in the 620–645 m section increases with depth, changing from −4.05 to −3.01, which corresponds to the domain of the sea-entry system. The $\delta^{26}Mg$ value of dolomite from 758.09 to 774.8 m section decreases with depth from −3.64 to −3.90, which corresponds to the high-level system domain; the dolomite $\delta^{26}Mg$ values of both sections from 1,063.46 to 1,109.77 m and from 1,159.77 to 1,179.62 m show a decreasing trend, as shown by the blue arrows in Figure 10, which

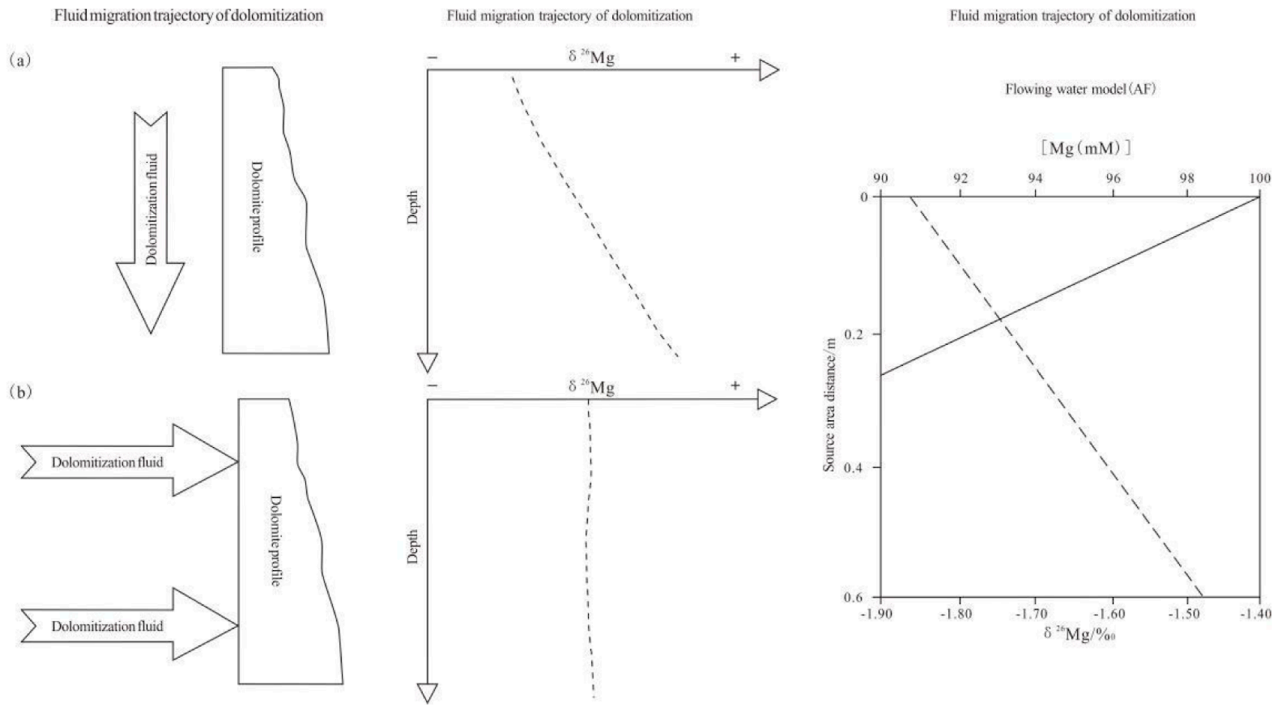

FIGURE 9
Simulation of Mg isotope fractionation during different dolomitization processes (modified after Ning et al., 2020): **(A)** Vertical downward migration of dolomitized fluids with δ^{26}Mg increasing with depth, mobile water model. **(B)** Lateral migration of dolomitized fluids, δ^{26}Mg remains constant with depth, and flowing water modeling.

corresponds well with the quasi-stratigraphic group of the dolomite sequence; from 1,063.46 to 1,109.77 m, the δ^{26}Mg value of dolomite decreased from −3.30 to −3.58, and from 1,159.77 to 1,179.62 m, the δ^{26}Mg value of dolomite decreased from −3.04 to −3.99.

The formation of shallow dolomite is subject to the joint action of atmospheric freshwater and seawater, and the biological remains are obvious. Dolomite particles are mostly developed at the edge of the holes; the particles are small and orderly at the bottom, dominated by powder crystals; most of them are straight-sided autoclave or semi-autoclave, and the mud crystal dolomite and powder crystal dolomite emit purple light. The dolomite δ^{26}Mg values in the 620–645-m section increase with depth, dolomitized fluids are transported vertically downward, and the flowing water model indicates a near-source backflow infiltration pattern. Dolomite grains with fog-centered bright rims are clearly characterized by incomplete dolomitization as fluid supply decreases in the lower portion, and calcite grains appear reddish under the stained thin sections. Dolomite particles still preferentially grow at the pore edges, but strongly dolomitized layer segments show a transition to semi-autonomous crystals due to recrystallization that squeezes the growth space. The δ^{26}Mg value of dolomite in the section from 758.09 to 774.8 m decreases with depth, indicating the upward migration of dolomitized fluids by hydrothermal fluids. The incomplete dolomitization of calcite in the upper part of the dolomite shows red color under the stained slice, and dolomite emits yellow and purple light due to the influence of manganese-bearing hydrothermal fluid, and the above two kinds of luminescent dolomite have the nature of ring-banded luminescence. The δ^{26}Mg values of dolomite in the two sections from 1,063.46 to 1,109.77 m and from 1,159.77 to 1,179.62 m show a decreasing trend, and the fine-crystalline dolomite mainly emits orange light with a small amount of violet light, and a small amount of dolomite is characterized by ring bands, but the ring bands are not obvious. Under the influence of hydrothermal fluid at the bottom, the fine-crystalline dolomite mainly emits orange-yellow light, with a small amount of orange-red light, and the orange-yellow light dolomite has a clear ring band.

4.4 Mechanisms of dolomitization

Multiple mechanisms of dolomitization are observed in Xisha biogenic reefs since reef formation. As mentioned earlier, different researchers have proposed different mechanisms from different perspectives. This study suggests that they are determined by the spatial variability of dolomitization fluids along the profile sequence since the formation of the reef and that there are three main mechanisms, namely, geothermal-driven, high-salt brine reflux and infiltration, as well as seawater-freshwater mixing. Of these, dolomitization is associated with periods of significant relative sea level decline (Wang et al., 2017).

Reflux infiltration mechanism is shown in Figure 11A.

It belongs to the quasi-syngenetic-shallow burial stage of diagenesis. The overall porosity and permeability of the Xike 1 well carbonate is good, with conditions for large-scale reflux permeable dolomitization. This stage is represented by strong metasomatism;

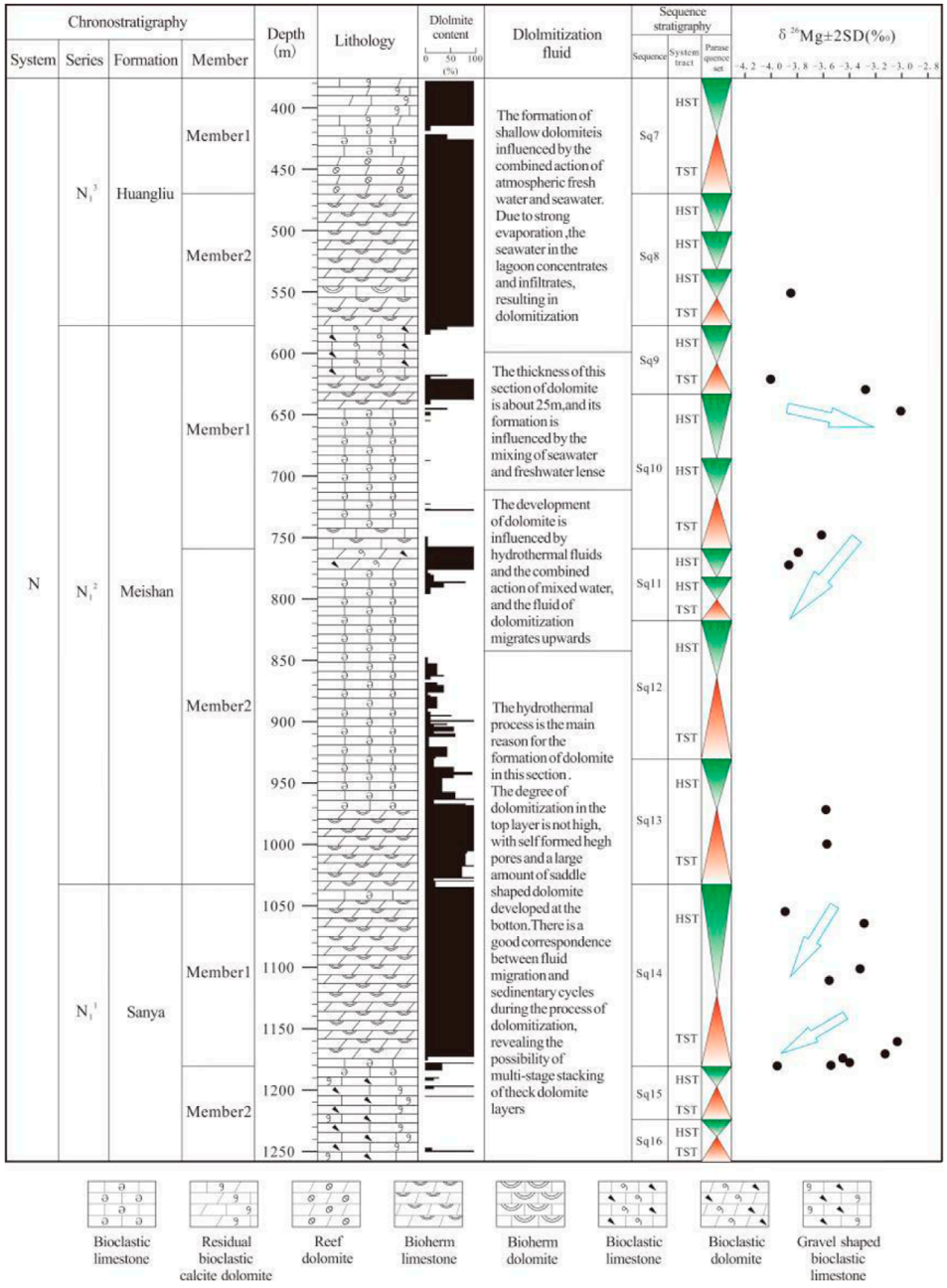

FIGURE 10
Vertical distribution characteristics of dolomitized fluids in the Xike 1 well (dolomite content referenced from Wang et al. (2020), stratigraphic data referenced from Liu et al. (2021). Blue arrows in the figure reflect δ^{26}Mg isotope trajectories in the direction of spatially varying fluid transport along the profile sequence).

dolomites are mainly powdery crystals, mostly face idiomorphic or semi-idiomorphic crystals, and the ordering degree is low. Microorganisms may also have influenced dolomite, with the development of dolomite on iron bacteria seen in the Xike 1 well.

Seawater concentrated by evaporation has relatively large δ^{18}O values, and sediments with δ18O greater than 2‰ form mainly in sedimentary media with higher than normal salinities. Wang et al. (2015) tested dolomite samples from the Huangliu Formation and the first member of the Meishan Formation in the Xike 1 well, and δ^{18}O was positive, with variations ranging from 2.293‰ to 5.072‰, and having an average value of 3.692‰. The δ^{18}O values of the dolomite are slightly higher, and the oxygen isotope values of the dolomite are generally indicative of the nature of the dolomite-forming fluid as slightly evaporated and concentrated seawater. The δ^{13}C varies from 1.214‰ to 3.051‰, with a mean value of 2.372‰; dolomite δ^{13}C and δ^{18}O show a significant positive correlation, indicating that the quasi-syncline was modified by atmospheric freshwater leaching and dissolution during the quasi-syncline.

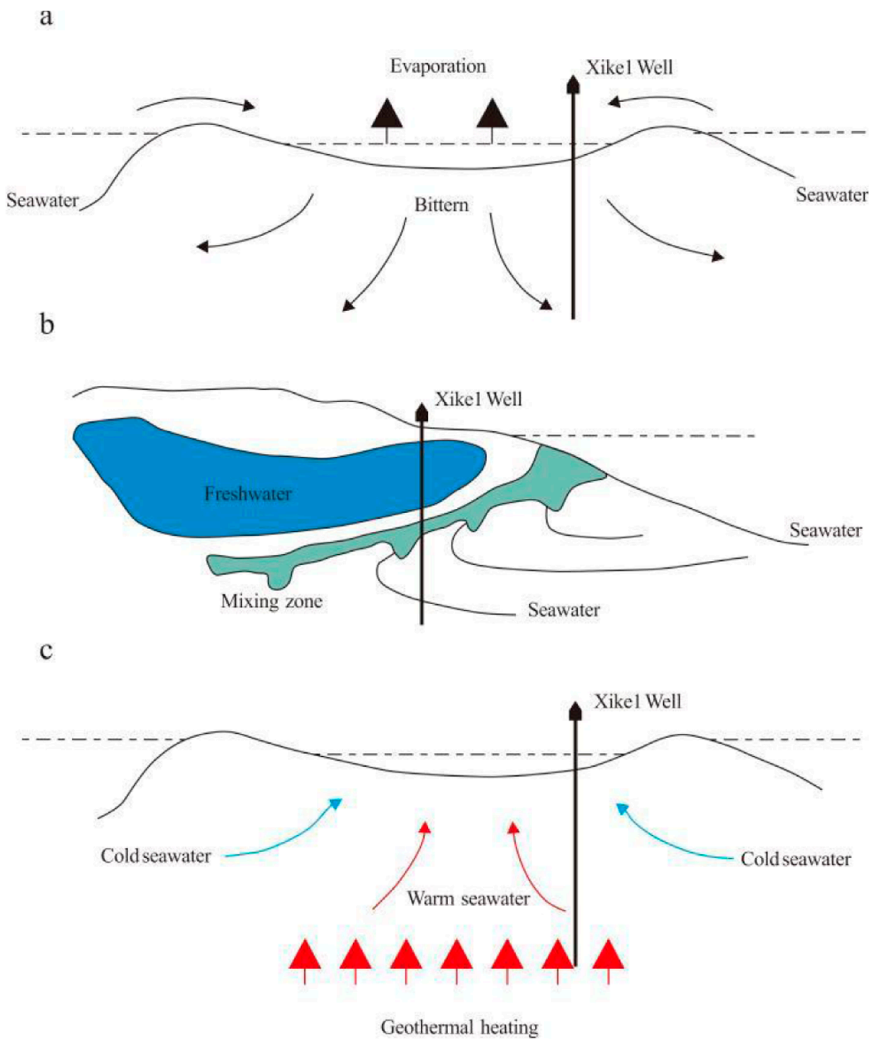

FIGURE 11
Dolomitization patterns of profile sequences in the study area. **(A)** Dolomitization occurs when seawater in the lagoon concentrates and seeps down as a result of strong evaporation. **(B)** Dolomitization in the mixed zone due to mixing of freshwater lenses and seawater. **(C)** Infiltration of warmer seawater into the overlying strata as a result of geothermal warming.

The δ^{26}Mg values of dolomite in the 620–645-m section increase with depth, the dolomitized fluids are transported vertically downward, and the flowing water model indicates a near-source backflow infiltration pattern. The Huangliu Formation dolomite lacks corresponding Mg isotope data, and it remains to be further verified whether δ^{26}Mg values vary with depth.

The mixed-water mechanism is shown in Figure 11B.

Freshwater lenses with a maximum thickness of <20 m (Zhou et al., 2006) are developed on Yongxing Island and Shi Island and are the only natural underground source of freshwater on Yongxing Island (Li et al., 2019). Rainwater infiltrated by the surface, due to the density difference with seawater, tends to form freshwater lenses underneath the atolls (Zhao and Wang, 2015) and forms a mixing zone between the seawater environments, in which the surrounding reefs are situated. Below the exposed surfaces of the Xisha islands, there is significant hydrochemical stratificationof freshwater and seawater, forming freshwater lenticular bodies, whereby mixed-water dolomitization occurs.

According to the actual data on the Xike 1 well, it is found that 4–5 dolomite wedges occur under the unconformity, which are individually a few meters thick, and the maximum thickness does not exceed 20 m. The mixed-water pattern is not the main reason for the development of thick-bedded dolomite in the area of the Xisha region.

The hydrothermal mechanism is shown in Figure 11C.

The rocky islands in Xisha have outcropping volcanic rocks, while the high pointed rocky islands are volcanic. The results of seismic data in the South China Sea and the region around Xisha Sea show that there has been strong volcanic activity in the northern waters of the South China Sea since the Late Miocene. Hydrothermal account of the process of dissolution, accompanied by the development of brecciated dolomite, its influence continues to the top of the second member of the Meishan Formation, the development of saddle-shaped dolomite, hydrothermal fluid

carrying Mn-bearing material to modify the dolomite, in particular, the second member of the Sanya Formation, the dolomite by the influence of the basement of the manganese-containing hydrothermal fluids cathodoluminescence under the ring band is obvious. Dong et al. (2021) confirmed that the deep dense dolomite fluids at the Xike 1 well are high-temperature hydrothermal fluids based on the measured fluid inclusion data. The low degree of dolomitization at the top of the microscopic dolomite section, the prevalence of incompletely dolomitized calcite, and the low degree of ordering all corroborate the possibility of hydrothermal upwelling.

The dolomite value of the 758.09~774.8-m section of the Xike 1 well decreases with depth, and the dolomite of the 1,063.46~1,109.77 m and 1,159.77~1,179.62-m sections shows a decreasing trend, respectively. This has a good correspondence with the dolomite sequence quasi-stratigraphic group and also directly indicates the hydrothermal upwelling action, which constitutes another class of dolomitization mechanism.

5 Conclusion

The formation mechanism of dolomite of the Xike 1 well in the Xisha Islands was investigated on the basis of the petrological and geochemical characterization of the core samples using experiments such as thin section identification, cathodoluminescence, scanning electron microscopy, electron microprobe, X-ray diffraction, and Mg isotope testing. The following conclusions can be drawn:

a) Dolomite is distributed along the weathering exposure surface. This dolomite mostly has a residual structure, while the dolomite without residual structures has a fog-centered bright edge, and the degree of authomorphism is controlled by the growth space, with straight authomorphism or semi-authomorphism, with the curved surface dominated.
b) The overall ordering of dolomite in the whole well is low, with an average value of 0.53, and there is little difference in ordering at different depths, the Mn and Fe contents of the middle and shallow-depth dolomites are generally low, and cathodoluminescence is not obvious, For the deep layers, the Mn and Fe contents increased by hydrothermal action, and bright yellow and orange cathodoluminescent bands were formed.
c) Changes in the Mg isotopic composition of dolomite along the stratigraphic sequence of the profile are generally consistent with changes in the depositional cycle. Based on the spatially varying trajectories of δ26Mg isotope profile sequences, the results indicate the presence of evaporative lagoon infiltration reflux, mixed water, and geothermally driven hydrothermal dolomitization mechanisms since reef formation.

Data availability statement

The original contributions presented in the study are included in the article/supplementary material; further inquiries can be directed to the corresponding author.

Author contributions

MY: conceptualization, data curation, formal analysis, investigation, methodology, software, validation, visualization, writing–original draft, and writing–review and editing. FH: data curation, formal analysis, methodology, software, validation, writing–original draft, and writing–review and editing. XH: data curation, formal analysis, methodology, software, validation, writing–original draft, and writing–review and editing. HZ: validation and writing–review and editing. LJ: validation and writing–review and editing. HC: supervision, validation, and writing–review and editing.

Funding

The author(s) declare that no financial support was received for the research and/or publication of this article.

Acknowledgments

The authors would like to show sincere thanks to all the technicians who have helped this research.

Conflict of interest

Author FH was employed by PetroChina Changqing Oilfield Company.

The remaining authors declare that the research was conducted in the absence of any commercial or financial relationships that could be construed as a potential conflict of interest.

Generative AI statement

The author(s) declare that no Generative AI was used in the creation of this manuscript.

Publisher's note

References

An, Y. J., Wu, F., Xiang, Y. X., Nan, X. Y., Huang, F., Yang, J., et al. (2014). High-precision Mg isotope analyses of low-Mg rocks by MC-ICP-MS. *Chem. Geol.* 390, 9–21. doi:10.1016/j.chemgeo.2014.09.014

Ashraf, U., Zhang, H., Anees, A., Ali, M., Mangi, H. N., and Zhang, X. (2024). An ensemble-based strategy for robust predictive volcanic rock typing efficiency on a global-scale: a novel workflow driven by big data analytics. *Sci. Total Environ.* 937, 173425. doi:10.1016/j.scitotenv.2024.173425

Ashraf, U., Zhang, H., Anees, A., Ali, M., Zhang, X., Shakeel Abbasi, S., et al. (2020). Controls on reservoir heterogeneity of a shallow-marine reservoir in sawan gas field, SE Pakistan: implications for reservoir quality prediction using acoustic impedance inversion. *Water* 12, 2972. doi:10.3390/w12112972

Ashraf, U., Zhang, H., Anees, A., Wang, R., Ali, M., Jiang, R., et al. (2022). Estimation of porosity and facies distribution through seismic inversion in an unconventional tight sandstone reservoir of Hangjinqi area, Ordos basin. *Front. Earth Sci.* 10. doi:10.3389/feart.2022.1014052

Cao, J. Q., Zhang, D. J., and Zhai, S. K. (2016). The characteristics and genetic model of the dolomitization in Xisha Reef Islands. *Haiyang Xuebao* 38, 125–139.

Dong, G., Liu, X. Y., Li, X. S., Zhang, D. J., Yan, G. J., Su, D. P., et al. (2021). Characteristics and diagenetic environment of tight dolostone in well Xike 1, south China sea. *Mar. Geol. Front.* 37, 49–54.

Dong, Z., Tian, S., Xue, H., Lu, S., Liu, B., Erastova, V., et al. (2024). Analysis of pore types in lower cretaceous qingshankou shale influenced by electric heating. *Energy and Fuels* 38, 20577–20590. doi:10.1021/acs.energyfuels.4c03783

Han, R., Zhang, Y., Wenlong, Q., Tianzhu, D., Mingzhi, W., and Feng, W. (2023). Geology and geochemistry of Zn-Pb(-Ge-Ag) deposits in the Sichuan-Yunnan-Guizhou Triangle area, China: a review and a new type. *Front. Earth Sci.* 11. doi:10.3389/feart.2023.1136397

Kaufman, A. J., Jacobsen, S. R., and Knoll, A. H. (1993). The Vendian record of Sr and C isotopic variations in seawater: implications for tectonics and paleoclimate. *Earth Planet Sci. Lett.* 120, 409–430. doi:10.1016/0012-821x(93)90254-7

Kaufman, A. J., and Knoll, A. H. (1995). Neoproterozoic variations in the C-isotopic composition of seawater: stratigraphic and biogeochemical implications. *Precambrian Res.* 73, 27–49. doi:10.1016/0301-9268(94)00070-8

Kouchinsky, A., Bengtson, S., Gallet, Y., Korovnikov, I., Pavlov, V., Runnegar, B., et al. (2008). The spice carbon isotope excursion in siberia: a combined study of the upper middle cambrian lowermost ordovician kulyumbe river section, northwestern siberian platform. *Geol. Mag.* 145, 609–622. doi:10.1017/s0016756808004913

Li, D., Ling, H. F., Jiang, S. Y., Pan, J. Y., Chen, Y. Q., Cai, Y. F., et al. (2009). New carbon isotope stratigraphy of the Ediacaran-Cambrian boundary interval from SW China: implications for global correlation. *Geol. Mag.* 146, 465–484. doi:10.1017/s0016756809006268

Li, D. N., Xu, J. X., Zhao, H., Chen, J., Sheng, C., and Chen, F. J. (2019). Temporal variations and influencing factors of freshwater lens in Yongxing Island. *J. Guangdong Ocean Univ.* 39, 67–74.

Li, X., Zhu, G. Y., Li, T. T., Zhou, L., Wu, Y. X., and Tian, L. J. (2022). Mg isotopic characteristics and genetic mechanism of dolomite of Cambrian Xixiangchi Formation in central Sichuan Basin. *Acta Pet. Sin.* 43, 1585–1603.

Lin, C., Deng, S., Mao, J., Jiang, Z., Chen, X., Yang, X., et al. (2024a). A new brittleness evaluation index for reservoir rocks based on fuzzy analytic hierarchy process and Energy dissipation. *SPE J.* 29, 5272–5285. doi:10.2118/223083-PA

Lin, C., Jia, X., Deng, S., Mao, J., Chen, X., He, J., et al. (2024b). The roles of micro pores and minerals in shale during hydraulic fracturing. *Rock Mech. Rock Eng.* 57, 10177–10186. doi:10.1007/s00603-024-04063-6

Liu, X. Y., Shao, L., Shi, D. F., Shi, W. F., and Ouyang, J. (2021). Element geochemistry of Well Xike 1 on the Xisha Islands and its bearing on sea level fluctuation. *Mar. Geol. Front.* 37, 8–17.

Luo, W., Zhang, D. J., Liu, X. Y., Wang, Z. F., Hu, W. Y., and Wang, Y. H. (2018). A comprehensive stratigraphic study of Well XK-1 in the Xisha area. *J. Stratigr.* 42, 485–498.

Ning, M., Huang, K. J., and Shen, B. (2018). Applications and advances of the magnesium isotope on the 'dolomite problem. *Acta Petrol. Sin.* 34, 3690–3708.

Ning, M., Lang, X. G., Huang, K. J., Huang, T., Yuan, H., Xing, C., et al. (2020). Towards understanding the origin of massive dolostones. *Earth Planet. Sci. Lett.* 545 (No), 116403. doi:10.1016/j.epsl.2020.116403

Richardson, M., Abraham-A, F., and Anthony, I. N. (2022). Physical properties of sandstone reservoirs: implication for fluid mobility. *Energy Geosci.* 3 (4), 349–359. doi:10.1016/j.engeos.2022.06.001

Shi, D. F., Li, X. Y., Wang, Y. H., Yin, H., Liu, J., Zhang, D. J., et al. (2010). Microbial characteristics of miocene dolomite in well xike-1, Xisha area, south China sea: implications for dolomitization. *Mineralogy Petrology* 40, 104–113.

Sibley, D. F., and Gregg, J. M. (1987). Classification of dolomite rock textures. *J. Sediment. Petrology* 57 (6), 967–975.

Tong, K., He, J., Dong, S., Sun, F., Chen, P., and Tong, Y. (2023). Fracture characterization of asmari formation carbonate reservoirs in G oilfield, zagros basin, Middle East. *Energy Geosci.* 4 (3), 100178–100210. doi:10.1016/j.engeos.2023.100178

Ullah, Z., Li, H., Khan, A., Faisal, S., Dilek, Y., Förster, M. W., et al. (2022). Mineralogy and PGE geochemistry of chromitites and peridotites of the sapat complex in the indus suture zone, northern Pakistan: implications for magmatic processes in the supra-subduction zone. *Int. Geol. Rev.* 65 (10), 1719–1744. doi:10.1080/00206814.2022.2106519

Wang, G. Z. (2001). Mixed sedimentation of recent reefoid carbonates and terrigenous clastics in the north continental shelf of the south China sea. *J. Palaeogeogr.* 2, 547–540. doi:10.7605/gdlxb.2001.02.006

Wang, R., Yu, K. F., Wang, Y. H., and Bian, L. Z. (2017). The diagenesis of coral reefs. *Adv. Earth Sci.* 32, 221–233.

Wang, X. R., Wang, Y. H., Liu, J., Zhang, D. J., Li, X. Y., and Shi, Z. Q. (2020). Characteristics and significance of manganese minerals in dolomite of Well Xike 1, Xisha area, South China SEA. *Mineralogy Petrology* 40, 81–91.

Wang, Z. F., Shi, Z. Q., Zhang, D. J., Huang, K. K., You, L., and Duan, X. (2015). Microscopic features and genesis for miocene to pliocene dolomite in Well Xike-1, Xisha Islands. *Earth Sci. J. China Univ. Geosciences* 40, 633–644. doi:10.3799/dqkx.2015.050

Wei, X., Jia, C. Z., and Meng, W. G. (2018). Dolomitization characteristics of carbonate rock in Xisha islands and its formation: a case study of Well Xichen-1. *J. Jilin Univ. Earth Sci. Ed.* 2, 217–224. doi:10.3969/j.issn.1671-5888.2008.02.006

Xie, R., Luo, Z., Zhang, M., Wang, Y., Chen, J., and Zhu, M. (2022). Factors controlling tight oil and gas reservoir development in the Jurassic siliciclastic-carbonate rocks in Sichuan Basin, China. *Energy Geosci.* 3 (4), 453–464. doi:10.1016/j.engeos.2021.08.001

Xiu, C., Zhang, D. J., Zhai, S. K., Liu, X. Y., Cao, J. Q., Bi, D. J., et al. (2017). REE geochemical characteristics and diagenetic environments of reef dolostone in Shi Island, Xisha Islands. *Mar. Sci. Bull.* 36, 151–159+167. doi:10.11840/j.issn.1001-6392.2017.02.005

Xu, H., Zhang, H. Y., Li, X. S., Shen, J. Y., Ma, X., Fu, H. P., et al. (2021). Geochemical behaviors and characteristics of iron isotope in the ferroan dolomite from Well Xiyong 2. *Mar. Geol. Front.* 37, 1–7.

Xu, H., Zhang, W. W., Wei, K., He, Q. K., Jiang, Y. S., Xu, T. T., et al. (2018). Ferroan dolomites in Miocene sediments of the Xisha Islands and their genetic model. *J. Oceanol. Limnol.* 36, 165–180. doi:10.1007/s00343-018-7136-3

Yang, L., Yang, D., L, i Y., Cai, J., Jiang, (2024). Nanoindentation study on microscopic mineral mechanics and bedding characteristics of continental shales. *Energy* 312, 133614. doi:10.1016/j.energy.2024.133614

Yin, H., Wang, Y. J., Liu, J., Shi, Z. Q., and Zhang, D. J. (2020). Characteristics and origin of dolostones in the miocene Meishan Formation in well Xike 1, Xisha islands, south China sea. *Oil and Gas Geol.* 41, 209–222.

Zhai, S. K., Mi, L. J., Shen, X., Liu, X. Y., Xiu, C., Sun, Z. P., et al. (2015). Mineral compositions and their environmental implications in reef of Shidao island, Xisha. *Earth Sci. J. China Univ. Geosciences.* 40, 597–605.

Zhao, H. T., and Wang, L. R. (2015). Review on the study of freshwater lens in the coral reef island. *Trop. Geogr.* 35, 120–129.

Zhou, C. Z., Fang, Z. D., Liang, H. G., Wang, H., and Ao, L. (2006). Influence of rainfall on freshwater lens in a coral island. *China Water and Wastewater* 1, 53–57. doi:10.1016/S1005-8885(07)60042-9

Zhu, W. L., Wang, Z. F., Mi, L. J., Du, X. B., Xie, X. N., Lu, Y. C., et al. (2015). Sequence stratigraphic framework and reef growth unit of well Xike-1 from Xisha Islands, South China Sea. *Earth Sci. J. China Univ. Geosciences* 40, 677–687. doi:10.3799/dqkx.2015.055